ACS APPLIED MATERIALS & INTERFACES

www.acsami.org

Research Article

Emergent Fabry–Pérot Interference for Light–Matter Interaction in van der Waals WS_2/SiP_2 Heterostructures

Xiaojun Sun,[‖] Feng Qin,[‖] Junwei Huang,[‖] Ling Zhou, Zeya Li, Xiangyu Bi, Lingyi Ao, Siyu Duan, Fanghua Cheng, Caiyu Qiu, Yangfan Lu, Hong Lu, Huiyang Gou, and Hongtao Yuan*

Cite This: *ACS Appl. Mater. Interfaces* 2022, 14, 7464–7470

Read Online

HPSTAR 1381-2022

ACCESS | Metrics & More | Article Recommendations | Supporting Information

ABSTRACT: Fabry–Pérot interference plays an important role in modulating the spectral intensity of optical response originating from light–matter interactions. Examples of such interference occurring in the substrate as the resonating cavity have been demonstrated and probed by two-dimensional layered materials. Similarly, the Fabry–Pérot interference can occur and modulate the optical response in the heterostructure; however, this remains elusive. Herein, we observe the Fabry–Pérot interference on photoluminescence (PL) and Raman spectra in monolayer WS_2/SiP_2 heterostructures by varying the thickness of bottom SiP_2 from 2 to 193 nm, which serves as the Fabry–Pérot cavity. Both the intensities of the PL spectra and the E^1_{2g} Raman mode of WS_2/SiP_2 heterostructures first decrease to almost zero while displaying an interference increase at a SiP_2 thickness of 75 nm. Our findings clearly demonstrate the Fabry–Pérot interference in the optical response of heterostructures, providing crucial information to optimize the optical response and paving the way toward photodetector applications.

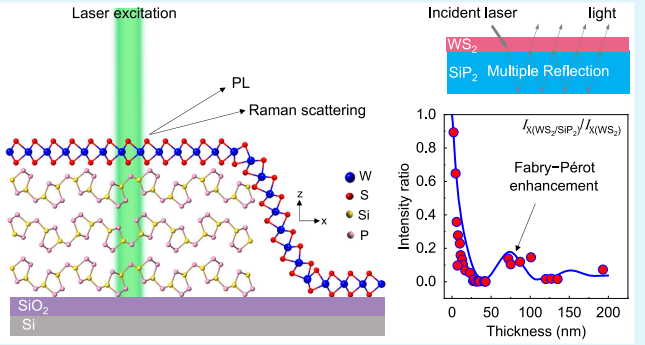

KEYWORDS: *Fabry–Pérot interference, two-dimensional materials, heterostructures, light–matter interaction, Raman, photoluminescence*

INTRODUCTION

The constructive and destructive interference originating from the light propagating between two parallel reflecting surfaces can cause resonance enhancement of the optical response, which is called Fabry–Pérot interference.[1−4] Examples can be found in monolayer transition metal dichalcogenides (TMDs) and graphene on the SiO_2 substrate with varying SiO_2 layer thickness,[5−9] in which the bottom SiO_2 can serve as a Fabry–Pérot cavity for resonating the incident light and resulting in the optimized optical response from monolayer TMDs. Based on the similar geometry in vertically stacked heterostructures,[10,11] the bottom materials should behave as the Fabry–Pérot cavity and thus are expected to affect the optical response of the top materials. When the thickness of the bottom material changes, the intensity of the PL and Raman spectra of the top material will change accordingly, resulting from constructive or destructive interference. Therefore, the Fabry–Pérot interference should play an important role in the optical response of heterostructures, providing crucial information for stacking heterostructures at proper thicknesses and for optimizing signals for potential applications. Similar to interesting optical physical mechanisms in heterostructures, including circularly polarized optical selection rules, moiré excitons, and optical generation of spin-valley currents,[12−18] the Fabry–Pérot interference can also modulate the spectral intensity and thus affect the optical response. However, such studies are rare, and the Fabry–Pérot interference in heterostructures remains elusive.

In this work, we demonstrate the effect of Fabry–Pérot interference on the PL and Raman spectra in monolayer WS_2/SiP_2 heterostructures. We found that the PL and Raman spectra of WS_2/SiP_2 heterostructures can be greatly tuned by the thickness of the bottom SiP_2 (the cavity thickness) and exhibit interference enhanced intensities at a specific intermediate thickness of SiP_2. Specifically, the PL intensity decreases with the increased thickness of SiP_2 from 2 to 50 nm and displays an interference enhancement when further increasing the thickness up to approximately 75 nm. Similarly, the intensity of the E^1_{2g} Raman mode of WS_2/SiP_2 heterostructures decreases with the increased thickness of SiP_2 and displays two interference enhancements with increased thickness. The intensity modulation of both the PL and Raman spectra of WS_2/SiP_2 heterostructures by changing

Received: November 23, 2021
Accepted: January 19, 2022
Published: January 31, 2022

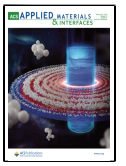

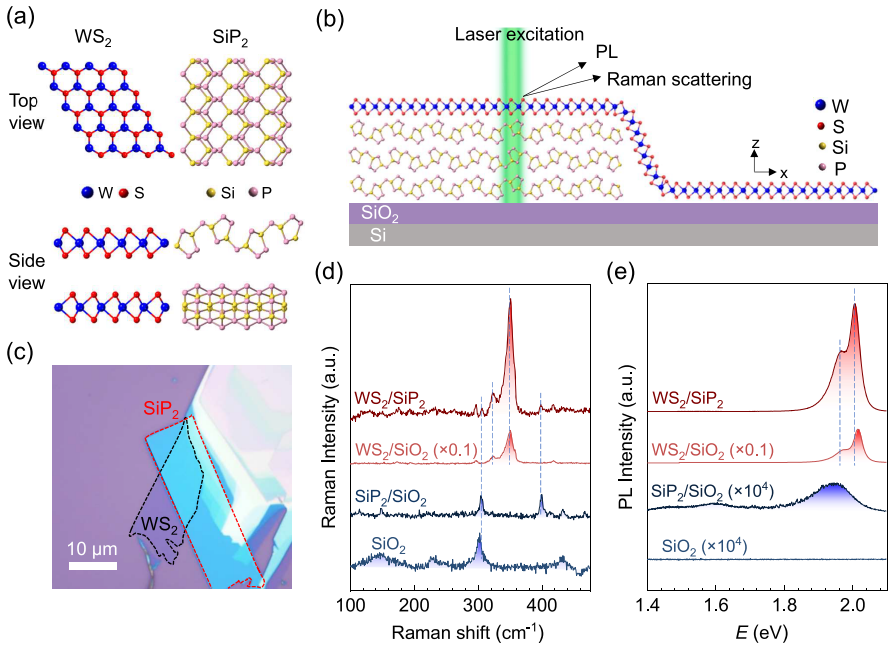

Figure 1. Raman and PL spectra of a monolayer WS_2/SiP_2 heterostructure. (a) Schematic crystal structure of WS_2 and SiP_2 in top and side views. (b) Schematic WS_2/SiP_2 heterostructure on SiO_2/Si substrates. (c) Microscopic optical image of the WS_2/SiP_2 heterostructure. WS_2 and SiP_2 flakes are marked with black and red dashed polygons, respectively. The Raman (d) and PL (e) spectra of SiO_2, SiP_2/SiO_2, monolayer WS_2/SiO_2, and monolayer WS_2/SiP_2 heterostructures.

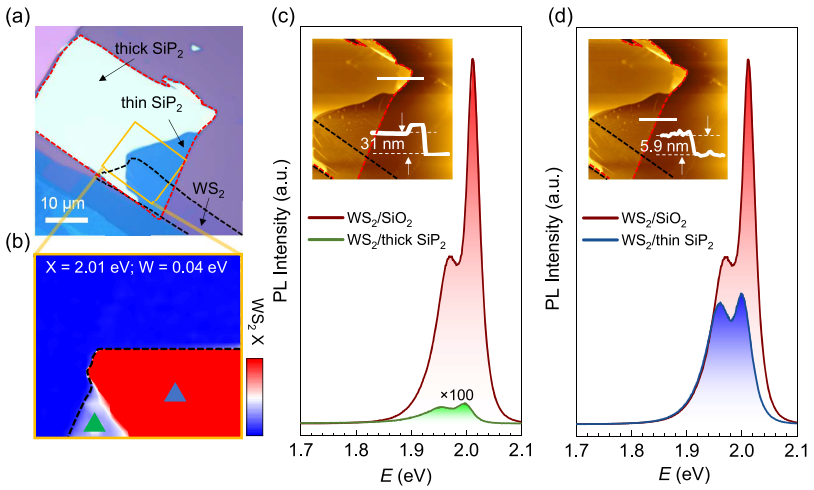

Figure 2. Comparison of monolayer WS_2/SiP_2 heterostructures with thick and thin SiP_2. (a) Microscopic optical image of WS_2/SiP_2 heterostructures. WS_2 and SiP_2 are marked with black and red dashed polygons, respectively. (b) Spatial distribution of the PL intensity within the region shown in the orange square in panel (a). (c, d) PL spectra of monolayer WS_2 on top of (c) thick and (d) thin SiP_2, as green and blue triangles marked in panel (b), respectively. Insets are the AFM topographies of WS_2/SiP_2 heterostructures, in which WS_2 and SiP_2 are marked with black and red dashed polygons, respectively. The thick and thin SiP_2 are identified to be 31.0 and 5.9 nm, respectively.

the thickness of SiP_2 gives us unambiguous evidence of the influence of Fabry–Pérot interference on the light–matter interactions in heterostructures, providing a quantitative reference for understanding the geometric effect in heterostructures and designing the thickness of cavity layers in heterostructures to optimize optical absorption in photodetector applications.

RESULTS AND DISCUSSION

To study the Fabry–Pérot interference effects on the light–matter interactions, we chose monolayer WS_2 (as the probing material) and SiP_2 (as the cavity material) to construct the heterostructures. On the one hand, monolayer WS_2 can present a relatively strong photoluminescence (left panel of Figure S1), which can easily analyze the changes in optical response caused by the Fabry–Pérot interference.[19−24] On the other hand, SiP_2 is also a van der Waals layered crystal (right panel of Figure 1a) and is easily exfoliated to show an atomically flat surface.[25] The atomically flat and clean interface between these two layered materials makes WS_2/SiP_2 heterostructures an ideal platform to study the effects of the Fabry–Pérot interference.

To compare the Fabry–Pérot interference effect with or without SiP_2, a part of the WS_2 monolayer is stacked above SiP_2 and the rest on the SiO_2/Si substrate. The cross-sectional schematic and microscopic optical picture of the monolayer

https://doi.org/10.1021/acsami.1c22768
ACS Appl. Mater. Interfaces 2022, 14, 7464−7470

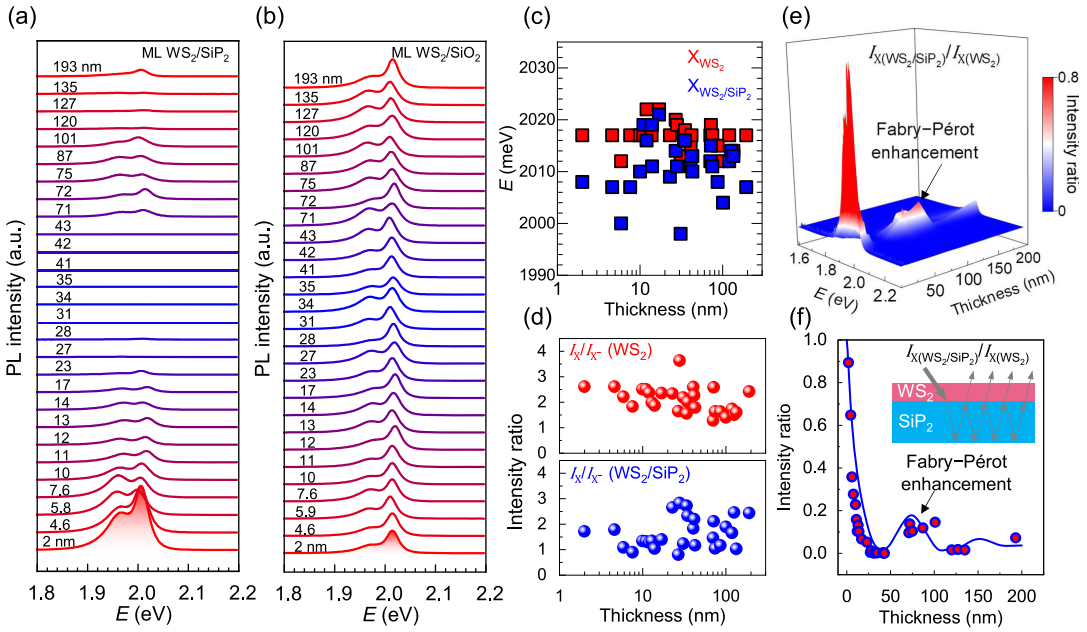

Figure 3. Fabry–Pérot interference of the PL spectra in monolayer WS_2/SiP_2 heterostructures. (a, b) Evolution of the PL spectra with the thickness of SiP_2 from 2 to 193 nm for (a) WS_2/SiP_2 heterostructures and (b) WS_2/SiO_2. (c) PL peak position of excitons (denoted as X) for WS_2 (red squares) and WS_2/SiP_2 heterostructures (blue squares) as a function of the thickness of SiP_2. (d) Intensity ratio of exciton (X) to trion (X^-) for WS_2 (upper panel) and WS_2/SiP_2 heterostructures (lower panel), respectively. (e) 3D color plot of the PL spectra of all the measured WS_2/SiP_2 heterostructures in panel (a). PL intensities are normalized by the intensity of the X peak in the corresponding PL spectra of monolayer WS_2 on SiO_2 in panel (b). (f) Normalized intensity of the X peak of WS_2/SiP_2 heterostructures as a function of the thickness of SiP_2. The inset shows a schematic mechanism of the Fabry–Pérot interference. A clear Fabry–Pérot enhancement is found when SiP_2 is 75 nm thick, as shown by the curve simulated.

WS_2/SiP_2 heterostructures are shown in Figure 1b and Figure 1c, respectively. Figure 1d presents the Raman spectra of the WS_2 monolayer, SiP_2 flake, and their heterostructure as well as the SiO_2 substrate, in which the Raman intensity of monolayer WS_2 is multiplied by 0.1. For the WS_2/SiP_2 heterostructure, the two Raman peaks located at 325 and 350 cm^{-1} are assigned to the in-plane $E^1_{2g}(M)$ and $E^1_{2g}(\Gamma)$ vibrational modes of monolayer WS_2, respectively, and the Raman peak at approximately 400 cm^{-1} originates from SiP_2, which is consistent with the previous Raman study.[25] These good agreements of the Raman peaks indicate the high quality of the WS_2/SiP_2 heterostructures, which is essential to study the Fabry–Pérot interference effect.

Figure 1e shows the PL spectra of monolayer WS_2, SiP_2, and their heterostructure, in which the PL intensity of monolayer WS_2 is multiplied by 0.1. For monolayer WS_2, the PL spectrum shows two characteristic peaks corresponding to the neutral exciton (X at 2.017 eV) and negatively charged exciton (X^- at 1.973 eV). The energy difference between the X and X^- peaks is 44 meV, which is the trion binding energy, reasonably coinciding with the reported trion dissociation energy.[26−28] As a comparison, for the WS_2/SiP_2 heterostructure, the X and X^- peaks redshift to lower energies at 2.007 and 1.967 eV, respectively. Such redshifts might originate from the change of the dielectric environment. When placing WS_2 onto SiP_2, the dielectric screening becomes stronger, which is expected to increase the strength of the Coulomb interaction in WS_2 and thus lead to an increase in the exciton binding energy of monolayer WS_2. With the assumption of a band gap value, the increased binding energy of WS_2 leads to a redshift of the PL spectrum. The explanations about the redshift have also been reported in the previous studies.[29−31] Notably, the intensities of both the Raman (Figure 1d) and PL (Figure 1e) spectra of monolayer WS_2 are weakened by the bottom SiP_2. The redshift of positions and the weakening of intensities of the PL peaks are independent of the measured locations on the sample surface, indicating the uniformity of our WS_2/SiP_2 heterostructures (further confirmed by the PL mapping measurements of WS_2/SiP_2 heterostructures in Figure S3).

To further study the weakening of intensity in the PL spectra, we fabricated a series of WS_2/SiP_2 heterostructures by altering the thickness of SiP_2. Figure 2a shows an optical image of the heterostructure, including a WS_2 monolayer stacked on a SiP_2 flake with different thicknesses, in which thicker (thinner) SiP_2 shows a pale white (blue) color, respectively. The thickness-dependent optical contrast of SiP_2 flakes is caused by Fabry–Pérot interference[32] within the flakes, which can be further confirmed by the colors of SiP_2 flakes with a series of thicknesses (Figure S4). Such an interference-determined color contrast has been well known in the fields of two-dimensional materials. To directly show the difference between the PL spectra of monolayer WS_2 on thick and thin SiP_2, we performed the spatial mapping of exciton X of the PL spectra, as shown in Figure 2b. The corresponding PL mapping of charged exciton X^- is shown in Figure S5. From the PL mapping results of X and X^-, one can see that the PL intensity of monolayer WS_2 is quite stable when the SiP_2 flake is homogeneous in thickness. As shown in Figure 2b, the PL emission intensity of monolayer WS_2 on thin SiP_2 is relatively stronger than that on thick SiP_2. This phenomenon is universal and does not depend on temperature, as shown in Figures S6 and S7, indicating that it has purely geometric origins.

Taking an example for better comparison, the PL spectra of monolayer WS_2 on thick and thin SiP_2 flakes are shown in

https://doi.org/10.1021/acsami.1c22768
ACS Appl. Mater. Interfaces 2022, 14, 7464−7470

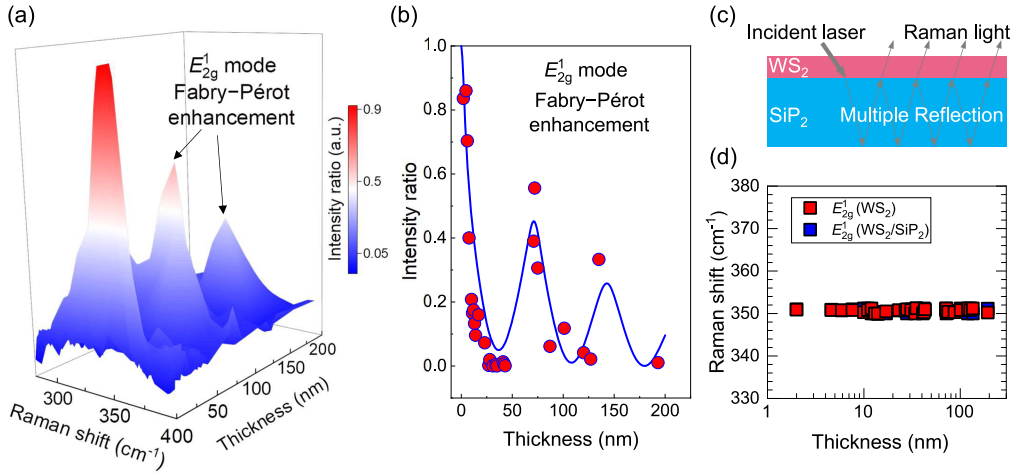

Figure 4. Fabry–Pérot interference of the Raman spectra in monolayer WS_2/SiP_2 heterostructures. (a) 3D color plot of the Raman spectra of all the measured WS_2/SiP_2 heterostructures. PL intensities are normalized by the intensity of the E^1_{2g} peak in the corresponding Raman spectra of monolayer WS_2 on SiO_2. (b) Raman intensity ratio of WS_2/SiP_2 heterostructures to monolayer WS_2, varying with the thickness of SiP_2. Two clear Fabry–Pérot enhancements are found when SiP_2 values are 75 and 140 nm in thickness, as shown by the simulated curve. (c) Schematic image of the optical paths of the excitation and Raman scattering light. (d) Raman peak position of the E^1_{2g} mode for WS_2 (red squares) and WS_2/SiP_2 heterostructures (blue squares) with different thicknesses of SiP_2.

Figure 2c and Figure 2d, respectively, in which the positions are marked by triangles in Figure 2b. The atomic force microscopy (AFM) images, as shown in the insets of Figure 2c,d, demonstrate that thick and thin SiP_2 flakes are uniform in thickness. The accurate thicknesses of SiP_2 are 31.0 and 5.9 nm, respectively, from the AFM results. Two important things should be addressed here. First, the PL intensities of WS_2/SiP_2 heterostructures with different thicknesses of SiP_2 are suppressed compared to those of monolayer WS_2 on the SiO_2 substrate. Second, the PL intensity of the WS_2/SiP_2 heterostructure with thinner SiP_2 (Figure 2d) is much stronger than that with thicker SiP_2 (Figure 2c). Such an intensity enhancement in the PL spectra of monolayer-WS_2/thinner-SiP_2 heterostructures suggests that a thick SiP_2 cavity has a higher light absorption rate than a thin cavity, which indicates the possible existence of the Fabry–Pérot interference effect in the SiP_2 cavity.

To further study the light–matter interactions influenced by the Fabry–Pérot interference in WS_2/SiP_2 heterostructures, we fabricated a series of monolayer WS_2/SiP_2 heterostructures with various thicknesses of bottom SiP_2 flakes from 2 to 193 nm and studied the thickness evolution of the PL and Raman spectra of top monolayer WS_2. Figure 3a,b compare the PL spectra of monolayer WS_2 on SiP_2 flakes with different thicknesses and the corresponding monolayer WS_2 on the SiO_2 substrate. Whether the bottom SiP_2 exists or not, monolayer WS_2 always displays two sharp PL peaks, namely, neutral exciton X and charged exciton X^-. Interestingly, WS_2/SiP_2 heterostructures present an obvious contrast in the intensity of the PL spectra with varying thickness of SiP_2, as shown in Figure 3a, which can be directly ascribed to the effect of Fabry–Pérot interference. However, all the WS_2 monolayers on the SiO_2 substrate corresponding to the heterostructures in Figure 3a present almost identical PL spectra in both intensity and peak positions, as shown in Figure 3b.

Intriguingly, two features in the PL spectra of WS_2/SiP_2 heterostructures should be addressed here. First, there is a redshift of the PL spectra of monolayer WS_2 on SiP_2 relative to that on the SiO_2 substrate. For example, the X peak of the PL spectra of monolayer WS_2/SiP_2 (Figure 3c) is located at approximately 2.008 eV, which is lower than those values (approximately 2.017 eV) on the SiO_2 substrate. Such a redshift in the PL spectra, indicating an increase in the exciton binding energy,[33] is mainly caused by the change in the dielectric environment from SiO_2 to SiP_2. Second, the intensity ratio of X and X^-, I_X/I_{X^-}, in WS_2/SiP_2 heterostructures shows a slight decreasing trend when thinning down SiP_2. Since I_X/I_{X^-} reflects the carrier density in monolayer WS_2, the changes of I_X/I_{X^-} in both monolayer WS_2 and WS_2/SiP_2 heterostructures provide crucial information on the charge transfer between WS_2 and SiP_2. As shown in Figure 3d, the values of I_X/I_{X^-} in monolayer WS_2 are approximately 2.5, while those in WS_2/SiP_2 heterostructures are slightly small, indicating that the carrier density of monolayer WS_2 on SiP_2 differs from that on SiO_2. Such a decrease in I_X/I_{X^-} in WS_2/SiP_2 heterostructures with reducing the thickness of SiP_2 corresponds to effective charge injection[28,34,35] into WS_2 and suggests the thickness dependence of the band structure of SiP_2. Such an observation that the dielectric environment can significantly affect the optical spectra of materials has also been frequently discussed in previous reports.[36−38]

More importantly, we discuss the effect of Fabry–Pérot interference in WS_2/SiP_2 heterostructures, which has been ignored in previous reports. Figure 3e plots the PL spectra of all the measured WS_2/SiP_2 heterostructures (Figure 3a), which are normalized by the intensity of the X peak in the corresponding PL spectra of monolayer WS_2 on SiO_2 (Figure 3b). This analysis is based on the fact that the exciton is directly related to the absorption and emission of monolayer WS_2. One can see in Figure 3e that the normalized PL spectra of WS_2/SiP_2 heterostructures are quickly suppressed with increasing SiP_2 thickness. A clear enhancement of the PL spectra appears when the thickness increases to a certain value. Figure 3f describes the normalized intensity of the X peak, which drops quickly from 0.9 down to almost zero with increasing thickness of SiP_2, enhances to ~0.2 when SiP_2 is 75

https://doi.org/10.1021/acsami.1c22768
ACS Appl. Mater. Interfaces 2022, 14, 7464−7470

nm thick, and decreases again to almost zero when further thickening SiP_2, evidently showing the constructive and deconstructive interference of absorption and emission of the light. The inset of Figure 3f schematically shows the coherent path of how the Fabry−Pérot interference within bottom SiP_2 affects the intensity of the PL spectra of top WS_2. In WS_2/SiP_2 heterostructures, the bottom SiP_2 behaves as a resonating cavity, in which the incident and emission light undergo an infinite number of reflections and refractions at the boundaries of both WS_2 and SiP_2 layers. Therefore, the Fabry−Pérot interference induced by SiP_2 can greatly affect the PL intensity and other light−matter interactions of WS_2, which is also confirmed in the plot of the peak area as a function of SiP_2 thickness, as shown in Figure S8a. The derivation and the full expressions of the simulated curve are given in Section S9 in the Supporting Information.

Similarly, the Fabry−Pérot interference of SiP_2 can also be proven by the Raman spectra of monolayer WS_2/SiP_2 heterostructures. One can see in Figure 4a that there are two enhanced peaks in the evolution of the Raman spectra with increasing SiP_2 thickness. To better understand these enhancements, Figure 4b profiles the normalized intensity of the E^1_{2g} peak as a function of the thickness of SiP_2, which drops quickly from ∼0.8 down to almost zero with increased thickness of SiP_2, then enhances twice to ∼0.6 and ∼0.4 when SiP_2 values are 75 and 140 nm in thickness, and eventually decreases to almost zero. The derivation and the full expressions of simulated curve are given in Section S9 in the Supporting Information. The optical path for the Fabry−Pérot interference effect on the Raman scattering process is schematically shown in Figure 4c, showing the constructive and deconstructive interference of the Raman scattering light. On the other hand, as shown in Figure 4d, one can see almost identical peak positions of the E^1_{2g} mode of monolayer WS_2 on either SiP_2 or SiO_2. As an intralayer vibration mode, the E^1_{2g} mode is sensitive to stress and shows redshifts or even splits as the stress increases.[39] The relative shift of the E^1_{2g} mode has not been found, proving that the observed two enhancements in the Raman spectra have purely geometric origins as the Fabry−Pérot interference, instead of the stress effect, which is possibly induced from the fabrication process.

CONCLUSIONS

In conclusion, by combining both PL and Raman measurements, we experimentally confirmed the influence of the Fabry−Pérot interference effect of SiP_2 on the optical response of WS_2/SiP_2 heterostructures. In these heterostructures, we found that both the PL and E^1_{2g} Raman peak intensities first decrease to almost zero as the SiP_2 thickness increases to 50 nm while displaying an interference enhancement at a SiP_2 thickness of approximately 75 nm. The Fabry−Pérot interference can be dramatically modulated by the thickness of SiP_2 and cause resonation of light focusing on specific layers. According to the simulation to experimental results, the thickness of SiP_2 at which the constructive and destructive interference of the light propagating through the SiP_2 layer can be quantitatively predicted. Fabry−Pérot interference is a common phenomenon that can occur when the ray passes through paired flats. Hence, the results can be generalized to any vertical two-dimensional material heterostructure, such as graphene, TMD, and phosphides. The simulation model can also be applied to these heterostructures for seeking the critical range of bottom material thickness and optimize the optical response. Our results introduce an interesting class of Fabry−Pérot interference enhancement in heterostructures, shedding light on the comprehensive understanding of the optical response of heterostructures. The potential of optimizing the optical response in heterostructures offers significant impacts for optoelectronic devices, including photodetectors, photovoltaics, and light-emitting devices with unprecedented characteristics or unique functionalities.

EXPERIMENTAL SECTION

Heterostructure Preparation. SiP_2 flakes with thicknesses varying from 2 to 193 nm were mechanically exfoliated onto silicon wafers with a 285 nm thick SiO_2 layer. Then, monolayer WS_2 was exfoliated using PDMS (polydimethylsiloxane), and the single layer was identified by the Raman spectroscopy characteristics. Eventually, monolayer WS_2 was transferred onto SiP_2. During the transfer process, a part of monolayer WS_2 was placed on the SiO_2 substrate for comparison to each other. All the exfoliation and transfer processes were performed in a nitrogen glove box with both oxygen and water levels below 0.1 ppm. After optical measurements, the thickness of SiP_2 was identified by atomic force microscopy (AFM, integrated onto the Raman system WITec Alpha 300).

Optical Measurements. Optical measurements, including the PL and Raman spectra, were performed by using a confocal Raman system (WITec Alpha 300). Thickness-dependent PL and Raman measurements were carried out at room temperature with an incident laser (a wavelength of 532 nm and laser power of 0.1 mW). The laser spot size is 1 μm focusing by using a 100× objective. Nitrogen ambient conditions were used to protect samples by continuously flowing nitrogen gas. Low-temperature PL measurements of heterostructures were performed under vacuum conditions with samples installed in a cryostat using a long working distance 50× objective with an incident laser (a wavelength of 532 nm and laser power of 0.1 mW). The cryostat was cooled with liquid nitrogen to provide a low-temperature platform for optical measurements.

ASSOCIATED CONTENT

Supporting Information

The Supporting Information is available free of charge at https://pubs.acs.org/doi/10.1021/acsami.1c22768.

The comparison of the PL intensity of WS_2, MoS_2, WSe_2, $MoSe_2$, and SiP_2; thickness information of the monolayer WS_2/SiP_2 heterostructure; PL intensity mapping of monolayer WS_2/SiP_2 heterostructures; color contrast of SiP_2 with different thicknesses and the PL spectra of their heterostructures with monolayer WS_2; the integrated PL intensity map of trion for WS_2/SiP_2 heterostructures; the PL mapping of WS_2/SiP_2 heterostructures with different thicknesses of SiP_2 at 300 K; the PL mapping of WS_2/SiP_2 heterostructures with different thicknesses of SiP_2 at 77 K; Fabry−Pérot interference enhancement confirmed by another definition; and analysis models for Fabry−Pérot interference (PDF)

AUTHOR INFORMATION

Corresponding Author

Hongtao Yuan − *College of Engineering and Applied Sciences, National Laboratory of Solid State Microstructures and Jiangsu Key Laboratory of Artificial Functional Materials, Nanjing University, Nanjing 210000, China*;
Email: htyuan@nju.edu.cn

https://doi.org/10.1021/acsami.1c22768
ACS Appl. Mater. Interfaces 2022, 14, 7464−7470

Authors

Xiaojun Sun − *College of Engineering and Applied Sciences, National Laboratory of Solid State Microstructures and Jiangsu Key Laboratory of Artificial Functional Materials, Nanjing University, Nanjing 210000, China;* orcid.org/0000-0002-7907-3426

Feng Qin − *College of Engineering and Applied Sciences, National Laboratory of Solid State Microstructures and Jiangsu Key Laboratory of Artificial Functional Materials, Nanjing University, Nanjing 210000, China;* orcid.org/0000-0003-0575-5691

Junwei Huang − *College of Engineering and Applied Sciences, National Laboratory of Solid State Microstructures and Jiangsu Key Laboratory of Artificial Functional Materials, Nanjing University, Nanjing 210000, China*

Ling Zhou − *College of Engineering and Applied Sciences, National Laboratory of Solid State Microstructures and Jiangsu Key Laboratory of Artificial Functional Materials, Nanjing University, Nanjing 210000, China*

Zeya Li − *College of Engineering and Applied Sciences, National Laboratory of Solid State Microstructures and Jiangsu Key Laboratory of Artificial Functional Materials, Nanjing University, Nanjing 210000, China*

Xiangyu Bi − *College of Engineering and Applied Sciences, National Laboratory of Solid State Microstructures and Jiangsu Key Laboratory of Artificial Functional Materials, Nanjing University, Nanjing 210000, China;* orcid.org/0000-0002-5344-3273

Lingyi Ao − *College of Engineering and Applied Sciences, National Laboratory of Solid State Microstructures and Jiangsu Key Laboratory of Artificial Functional Materials, Nanjing University, Nanjing 210000, China*

Siyu Duan − *College of Engineering and Applied Sciences, National Laboratory of Solid State Microstructures and Jiangsu Key Laboratory of Artificial Functional Materials, Nanjing University, Nanjing 210000, China*

Fanghua Cheng − *College of Engineering and Applied Sciences, National Laboratory of Solid State Microstructures and Jiangsu Key Laboratory of Artificial Functional Materials, Nanjing University, Nanjing 210000, China*

Caiyu Qiu − *College of Engineering and Applied Sciences, National Laboratory of Solid State Microstructures and Jiangsu Key Laboratory of Artificial Functional Materials, Nanjing University, Nanjing 210000, China*

Yangfan Lu − *College of Materials Science and Engineering, National Engineering Research Center for Magnesium Alloys, Chongqing University, Chongqing 400030, China;* orcid.org/0000-0003-2084-9549

Hong Lu − *College of Engineering and Applied Sciences, National Laboratory of Solid State Microstructures and Jiangsu Key Laboratory of Artificial Functional Materials, Nanjing University, Nanjing 210000, China;* orcid.org/0000-0002-8340-2739

Huiyang Gou − *Center for High Pressure Science and Technology Advanced Research, Beijing 100094, China;* orcid.org/0000-0002-2612-4314

Complete contact information is available at: https://pubs.acs.org/10.1021/acsami.1c22768

Author Contributions

[‖]X.S., F.Q., and J.H. contributed equally to this work. H.T.Y. conceived the project and designed the experiments. X.S., X.B., L.Z., and Z.L. prepared the devices. X.S., L.Z., F.Q., and J.H. carried out the optical measurements. H.G. and Y.L. prepared the SiP_2 single crystal. X.S., L.A., S.D., F.C., and C.Q. discussed and analyzed the experimental data. X.S., F.Q., and H.T.Y. wrote the manuscript with input from all authors.

Notes

The authors declare no competing financial interest.

■ ACKNOWLEDGMENTS

This research was supported by the National Natural Science Foundation of China (91750101, 21733001, 52072168, and 51861145201), the National Key Basic Research Program of the Ministry of Science and Technology of China (2018YFA0306200), the Fundamental Research Funds for the Central Universities (021314380078, 021314380104, and 021314380147), and Jiangsu Key Laboratory of Artificial Functional Materials. Y.L. acknowledges financial support from the start-up fund of Chongqing University (02110011044171).

■ REFERENCES

(1) Kats, M. A.; Blanchard, R.; Genevet, P.; Capasso, F. Nanometre Optical Coatings Based on Strong Interference Effects in Highly Absorbing Media. *Nat. Mater.* **2013**, *12*, 20−24.

(2) Yan, R. H.; Simes, R. J.; Coldren, L. A. Electroabsorptive Fabry-Perot Reflection Modulators with Asymmetric Mirrors. *IEEE Photonics Technol. Lett.* **1989**, *1*, 273−275.

(3) Faist, J.; Capasso, F.; Sirtori, C.; West, K. W.; Pfeiffer, L. N. Controlling the Sign of Quantum Interference by Tunnelling from Quantum Wells. *Nature* **1997**, *390*, 589−591.

(4) Liang, W.; Bockrath, M.; Bozovic, D.; Hafner, J. H.; Tinkham, M.; Park, H. Fabry-Perot Interference in a Nanotube Electron Waveguide. *Nature* **2001**, *411*, 665−669.

(5) Lu, Y.; Li, X.-L.; Zhang, X.; Wu, J.-B.; Tan, P.-H. Optical Contrast Determination of the Thickness of SiO_2 Film on Si Substrate Partially Covered by Two-Dimensional Crystal Flakes. *Sci. Bull.* **2015**, *60*, 806−811.

(6) Huang, L.; Shang, Z.; Gao, M.; Miao, C.; Cheng, Y.; Huang, W. Optimized Parameters for Identifying the Layer Number of Few Layer Chromium Tri-Iodide from a Theoretical Perspective: Implications for Two-Dimensional Spintronics. *ACS Appl. Nano Mater.* **2020**, *3*, 8382−8388.

(7) Li, X. L.; Qiao, X. F.; Han, W. P.; Lu, Y.; Tan, Q. H.; Liu, X. L.; Tan, P. H. Layer Number Identification of Intrinsic and Defective Multilayered Graphenes up to 100 Layers by the Raman Mode Intensity from Substrates. *Nanoscale* **2015**, *7*, 8135−8141.

(8) Zhang, H.; Wan, Y.; Ma, Y.; Wang, W.; Wang, Y.; Dai, L. Interference Effect on Optical Signals of Monolayer MoS_2. *Appl. Phys. Lett.* **2015**, *107*, 101904.

(9) Li, S. L.; Miyazaki, H.; Song, H.; Kuramochi, H.; Nakaharai, S.; Tsukagoshi, K. Quantitative Raman Spectrum and Reliable Thickness Identification for Atomic Layers on Insulating Substrates. *ACS Nano* **2012**, *6*, 7381−7388.

(10) Novoselov, K. S.; Mishchenko, A.; Carvalho, A.; Castro Neto, A. H. 2D Materials and van der Waals Heterostructures. *Science* **2016**, *353*, 9439.

(11) Jariwala, D.; Marks, T. J.; Hersam, M. C. Mixed-Dimensional van der Waals Heterostructures. *Nat. Mater.* **2017**, *16*, 170−181.

(12) Hsu, W. T.; Lu, L. S.; Wu, P. H.; Lee, M. H.; Chen, P. J.; Wu, P. Y.; Chou, Y. C.; Jeng, H. T.; Li, L. J.; Chu, M. W.; Chang, W. H. Negative Circular Polarization Emissions from $WSe_2/MoSe_2$ Commensurate Heterobilayers. *Nat. Commun.* **2018**, *9*, 1356.

(13) Rivera, P.; Yu, H.; Seyler, K. L.; Wilson, N. P.; Yao, W.; Xu, X. Interlayer Valley Excitons in Heterobilayers of Transition Metal Dichalcogenides. *Nat. Nanotechnol.* **2018**, *13*, 1004−1015.

(14) Liu, Y.; Rodrigues, J. N. B.; Luo, Y. Z.; Li, L.; Carvalho, A.; Yang, M.; Laksono, E.; Lu, J.; Bao, Y.; Xu, H.; Tan, S. J. R.; Qiu, Z.; Sow, C. H.; Feng, Y. P.; Neto, A. H. C.; Adam, S.; Lu, J.; Loh, K. P.

Tailoring Sample-Wide Pseudo-Magnetic Fields on a Graphene-Black Phosphorus Heterostructure. *Nat. Nanotechnol.* **2018**, *13*, 828−834.
(15) Zhao, W.; Regan, E. C.; Wang, D.; Jin, C.; Hsieh, S.; Wang, Z.; Wang, J.; Wang, Z.; Yumigeta, K.; Blei, M.; Watanabe, K.; Taniguchi, T.; Tongay, S.; Yao, N. Y.; Wang, F. Dynamic Tuning of Moiré Excitons in a WSe_2/WS_2 Heterostructure via Mechanical Deformation. *Nano Lett.* **2021**, *21*, 8910−8916.
(16) Tran, K.; Moody, G.; Wu, F.; Lu, X.; Choi, J.; Kim, K.; Rai, A.; Sanchez, D. A.; Quan, J.; Singh, A.; Embley, J.; Zepeda, A.; Campbell, M.; Autry, T.; Taniguchi, T.; Watanabe, K.; Lu, N.; Banerjee, S. K.; Silverman, K. L.; Kim, S.; Tutuc, E.; Yang, L.; MacDonald, A. H.; Li, X. Evidence for Moiré Excitons in van der Waals Heterostructures. *Nature* **2019**, *567*, 71−75.
(17) Cho, C.; Wong, J.; Taqieddin, A.; Biswas, S.; Aluru, N. R.; Nam, S.; Atwater, H. A. Highly Strain-Tunable Interlayer Excitons in MoS_2/WSe_2 Heterobilayers. *Nano Lett.* **2021**, *21*, 3956−3964.
(18) Akamatsu, T.; Ideue, T.; Zhou, L.; Dong, Y.; Kitamura, S.; Yoshii, M.; Yang, D. Y.; Onga, M.; Nakagawa, Y.; Watanabe, K.; Taniguchi, T.; Laurienzo, J.; Huang, J. W.; Ye, Z. L.; Morimoto, T.; Yuan, H. T.; Iwasa, Y. A van der Waals Interface That Creates In-Plane Polarization and a Spontaneous Photovoltaic Effect. *Science* **2021**, *372*, 68−72.
(19) Schüler, M.; Giovannini, U. D.; Hübener, H.; Rubio, A.; Sentef, M. A.; Werner, P. Local Berry Curvature Signatures in Dichroic Angle-Resolved Photoelectron Spectroscopy from Two-Dimensional Materials. *Sci. Adv.* **2020**, *6*, 2730.
(20) Splendiani, A.; Sun, L.; Zhang, Y.; Li, T.; Kim, J.; Chim, C. Y.; Galli, G.; Wang, F. Emerging Photoluminescence in Monolayer MoS_2. *Nano Lett.* **2010**, *10*, 1271−1275.
(21) Mak, K. F.; Lee, C.; Hone, J.; Shan, J.; Heinz, T. F. Atomically Thin MoS_2: A New Direct-Gap Semiconductor. *Phys. Rev. Lett.* **2010**, *105*, 136805.
(22) Meunier, V.; Lambin, P.; Lucas, A. A. Atomic and Electronic Structures of Large and Small Carbon Tori. *Phys. Rev. B* **1998**, *57*, 14886−14890.
(23) Islam, M. R.; Kang, N.; Bhanu, U.; Paudel, H. P.; Erementchouk, M.; Tetard, L.; Leuenberger, M. N.; Khondaker, S. I. Tuning the Electrical Property via Defect Engineering of Single Layer MoS_2 by Oxygen Plasma. *Nanoscale* **2014**, *6*, 10033−10039.
(24) Stoica, V. A.; Laanait, N.; Dai, C.; Hong, Z.; Yuan, Y.; Zhang, Z.; Lei, S.; McCarter, M. R.; Yadav, A.; Damodaran, A. R.; Das, S.; Stone, G. A.; Karapetrova, J.; Walko, D. A.; Zhang, X.; Martin, L. W.; Ramesh, R.; Chen, L. Q.; Wen, H.; Gopalan, V.; Freeland, J. W. Optical Creation of a Supercrystal with Three-Dimensional Nanoscale Periodicity. *Nat. Mater.* **2019**, *18*, 377−383.
(25) Zhang, X.; Wang, S.; Ruan, H.; Zhang, G.; Tao, X. Structure and Growth of Single Crystal SiP_2 Using Flux Method. *Solid State Sci.* **2014**, *37*, 1−5.
(26) Del Corro, E.; Botello-Mendez, A.; Gillet, Y.; Elias, A. L.; Terrones, H.; Feng, S.; Fantini, C.; Rhodes, D.; Pradhan, N.; Balicas, L.; Gonze, X.; Charlier, J. C.; Terrones, M.; Pimenta, M. A. Atypical Exciton-Phonon Interactions in WS_2 and WSe_2 Monolayers Revealed by Resonance Raman Spectroscopy. *Nano Lett.* **2016**, *16*, 2363−2368.
(27) Lee, Y.; Ghimire, G.; Roy, S.; Kim, Y.; Seo, C.; Sood, A. K.; Jang, J. I.; Kim, J. Impeding Exciton-Exciton Annihilation in Monolayer WS_2 by Laser Irradiation. *ACS Photonics* **2018**, *5*, 2904−2911.
(28) Mak, K. F.; He, K.; Lee, C.; Lee, G. H.; Hone, J.; Heinz, T. F.; Shan, J. Tightly Bound Trions in Monolayer MoS_2. *Nat. Mater.* **2013**, *12*, 207−211.
(29) Florian, M.; Hartmann, M.; Steinhoff, A.; Klein, J.; Holleitner, A. W.; Finley, J. J.; Wehling, T. O.; Kaniber, M.; Gies, C. The Dielectric Impact of Layer Distances on Exciton and Trion Binding Energies in van der Waals Heterostructures. *Nano Lett.* **2018**, *18*, 2725−2732.
(30) Ugeda, M. M.; Bradley, A. J.; Shi, S. F.; da Jornada, F. H.; Zhang, Y.; Qiu, D. Y.; Ruan, W.; Mo, S. K.; Hussain, Z.; Shen, Z. X.; Wang, F.; Louie, S. G.; Crommie, M. F. Giant Bandgap Renormalization and Excitonic Effects in a Monolayer Transition Metal Dichalcogenide Semiconductor. *Nat. Mater.* **2014**, *13*, 1091−1095.
(31) Raja, A.; Chaves, A.; Yu, J.; Arefe, G.; Hill, H. M.; Rigosi, A. F.; Berkelbach, T. C.; Nagler, P.; Schuller, C.; Korn, T.; Nuckolls, C.; Hone, J.; Brus, L. E.; Heinz, T. F.; Reichman, D. R.; Chernikov, A. Coulomb Engineering of the Bandgap and Excitons in Two-Dimensional Materials. *Nat. Commun.* **2017**, *8*, 15251.
(32) Castellanos-Gomez, A.; Agraät, N.; Rubio-Bollinger, G. Optical Identification of Atomically Thin Dichalcogenide Crystals. *Appl. Phys. Lett.* **2010**, *96*, 213116.
(33) Jadczak, J.; Bryja, L.; Kutrowska-Girzycka, J.; Kapuscinski, P.; Bieniek, M.; Huang, Y. S.; Hawrylak, P. Room Temperature Multi-Phonon Upconversion Photoluminescence in Monolayer Semiconductor WS_2. *Nat. Commun.* **2019**, *10*, 107.
(34) Mouri, S.; Miyauchi, Y.; Matsuda, K. Tunable Photoluminescence of Monolayer MoS_2 via Chemical Doping. *Nano Lett.* **2013**, *13*, 5944−5948.
(35) Omar, S.; van Wees, B. J. Graphene-WS_2 Heterostructures for Tunable Spin Injection and Spin Transport. *Phys. Rev. B* **2017**, *95*, No. 081404.
(36) Liu, W.; Kang, J.; Sarkar, D.; Khatami, Y.; Jena, D.; Banerjee, K. Role of Metal Contacts in Designing High-Performance Monolayer n-type WSe_2 Field Effect Transistors. *Nano Lett.* **2013**, *13*, 1983−1990.
(37) Borghardt, S.; Tu, J.-S.; Winkler, F.; Schubert, J.; Zander, W.; Leosson, K.; Kardynał, B. E. Engineering of Optical and Electronic Band Gaps in Transition Metal Dichalcogenide Monolayers Through External Dielectric Screening. *Phys. Rev. Mater.* **2017**, *1*, No. 054001.
(38) Cho, K.; Pak, J.; Chung, S.; Lee, T. Recent Advances in Interface Engineering of Transition-Metal Dichalcogenides with Organic Molecules and Polymers. *ACS Nano* **2019**, *13*, 9713−9734.
(39) Zhu, C. R.; Wang, G.; Liu, B. L.; Marie, X.; Qiao, X. F.; Zhang, X.; Wu, X. X.; Fan, H.; Tan, P. H.; Amand, T.; Urbaszek, B. Strain Tuning of Optical Emission Energy and Polarization in Monolayer and Bilayer MoS_2. *Phys. Rev. B* **2013**, *88*, 121301.

https://doi.org/10.1021/acsami.1c22768
ACS Appl. Mater. Interfaces 2022, 14, 7464−7470